

Highlighting research from Prof. Namrata Gundiah's group at the Biomechanics Laboratory, Indian Institute of Science, Bangalore.

Traction cytometry: regularization in the Fourier approach and comparisons with finite element method

A brightfield image of a cell on a polyacrylamide substrate with fluorescent beads was obtained. Deformed and referential configurations of beads in the presence and absence of the cell were used to calculate gel displacements. Tractions, computed using the finite element method and Fourier transform traction cytometry with regularization, were compared. Nodal force maps show spatial distribution of forces at adhesions.

As featured in:



See Namrata Gundiah et al.,
Soft Matter, 2018, 14, 4687.



Cite this: *Soft Matter*, 2018,
14, 4687

Traction cytometry: regularization in the Fourier approach and comparisons with finite element method[†]

Ankur H. Kulkarni,[‡]^a Prasenjit Ghosh,^{ID}[‡]^b Ashwin Seetharaman,^b Paturu Kondaiah^a and Namrata Gundiah^{ID}^{*}^b

Traction forces exerted by adherent cells are quantified using displacements of embedded markers on polyacrylamide substrates due to cell contractility. Fourier Transform Traction Cytometry (FTTC) is widely used to calculate tractions but has inherent limitations due to errors in the displacement fields; these are mitigated through a regularization parameter (γ) in the Reg-FTTC method. An alternate finite element (FE) approach computes tractions on a domain using known boundary conditions. Robust verification and recovery studies are lacking but essential in assessing the accuracy and noise sensitivity of the traction solutions from the different methods. We implemented the L2 regularization method and defined a maximum curvature point in the traction with γ plot as the optimal regularization parameter (γ^*) in the Reg-FTTC approach. Traction reconstructions using γ^* yield accurate values of low and maximum tractions (T_{\max}) in the presence of up to 5% noise. Reg-FTTC is hence a clear improvement over the FTTC method but is inadequate to reconstruct low stresses such as those at nascent focal adhesions. FE, implemented using a node-by-node comparison, showed an intermediate reconstruction compared to Reg-FTTC. We performed experiments using mouse embryonic fibroblast (MEF) and compared results between these approaches. Tractions from FTTC and FE showed differences of ~92% and 22% as compared to Reg-FTTC. Selection of an optimum value of γ for each cell reduced variability in the computed tractions as compared to using a single value of γ for all the MEF cells in this study.

Received 10th November 2017,
Accepted 27th April 2018

DOI: 10.1039/c7sm02214j

rsc.li/soft-matter-journal

Introduction

Traction forces are used to quantify interactions between cells and the underlying substrate and are important in cellular adhesion and migration.^{1–3} Cells respond to changes in their mechanical milieu through a dynamic feedback involving focal adhesions and cytoskeletal proteins.^{4,5} Linear elastic gels, such as polyacrylamide (PA), are generally used to relate the surface displacements to tractions on an elastic semi-infinite gel using a linear elasticity Boussinesq–Cerruti formulation.⁶ In this method, the in-plane displacement field caused by cell contractions on the free surface is represented as a convolution integral of the Green's function and the in-plane traction field. This inverse approach to calculate tractions is a Fredholm integral of the first kind that is inherently ill-posed and highly sensitive to noise in the input displacement data. Butler *et al.* solved the Fredholm integral

equations in Fourier space and introduced a highly efficient Fourier Transform Traction Cytometry (FTTC) method that is routinely used to report cell traction forces on a discretized domain of in-plane displacements.⁷ Lin *et al.* investigated the influence of the substrate thickness on the measured forces exerted by the cell in the FTTC method; the forces varied significantly as the substrate thickness approached the lateral dimensions of the cell.⁸ The FTTC method however suffers from drawbacks due to smoothening of the traction outputs which results in amplification of higher spatial frequencies. Schwarz and co-workers emphasized the need for regularization in FTTC and employed a zeroth-order Tikhonov regularization of FTTC (Reg-FTTC) to mitigate these effects and obtain stable solutions through the point force method.⁹ Regularization is essentially a compromise between the accuracy and stability of the solution: a strongly regularized solution may result in poor approximations of traction. In contrast, a weakly regularized solution suffers from stability issues that are inherent in the inverse method. Determination of an optimum level of regularization is currently based on subjective judgements that depend on the magnitude of exerted traction and the extent of localization which is achieved with a single value regularization parameter for all cells.⁹ Han and co-workers implemented an L1 regularization

^a Department of Molecular Reproduction, Development and Genetics,
Indian Institute of Science, Bangalore 560012, India

^b Department of Mechanical Engineering, Indian Institute of Science,
Bangalore 560012, India. E-mail: namrata@iisc.ac.in, ngundiah@gmail.com

† Electronic supplementary information (ESI) available. See DOI: 10.1039/c7sm02214j

‡ Equal contribution

method to improve the stress reconstructions at nascent focal adhesions (NA) based on the inverse approach.¹⁰ They showed an improvement in the magnitude and fidelity of low stress reconstructions in the NA regions without the constraining effects in the point force method.⁹ The L1 regularization is however computationally expensive; albeit it has also been recently used to compute tractions for the entire cell.¹¹

An alternative approach to the Boussinesq–Cerruti formulation is to solve for the unknown tractions on a finite-sized substrate through a boundary-value problem using a numerical finite element (FE) method. The discretized FE domain has a stiffness matrix which is a function of the material and geometric properties of the underlying substrate. A distinct advantage is that the matrix is well-conditioned for a rectangular block with regular discretization; its inversion hence yields stable solutions. The boundary conditions at every point of the domain boundary are completely specified either in terms of the known tractions or the known displacements along each orthogonal direction. Earlier studies implemented mesh convergence checks on average measures of the stress field to assess the effect of discretization on results from FE simulations.^{12–14} Use of average output criteria in assessing convergence may not be sufficient to estimate the solution accuracy. A convergence procedure which considers discretization-induced variation in stresses across the domain should be explored to better reflect the solution errors. Differences in employing direct or inverse mathematical approaches may result in variability in reporting cellular tractions. Verification methods using simulated loads to compute differences in predicted tractions between the different approaches are essential to assess the fidelity of reconstructions and robustness of the different approaches.

We used a verification method based on displacements corresponding to prescribed loads at known positions on a linear elastic gel and computed tractions using the FTTC, Reg-FTTC, and FE methods. We performed a sensitivity analysis in the presence of simulated displacement noise and used a node-by-node evaluation to compare traction metrics. Our studies highlight the inherent stability problems in the FTTC method that may be mitigated using the regularized approach to recover low forces. Results from the FE simulations had an intermediate traction reconstruction as compared to those from the Fourier approaches. We also performed experimental measurements using mouse epithelial fibroblasts adherent on polyacrylamide gels. Results from our study show significant differences in the reported traction outputs from FTTC, Reg-FTTC, and FE approaches which follow the trends in the simulated study. Because Reg-FTTC is highly sensitive to the choice of regularization parameter, we explored methods to aid in the selection of an optimum value of regularization for each cell. This approach reduces the variability in reported tractions when using the Reg-FTTC approach. Comparative approaches are essential to accurately and reliably quantify the heterogeneity, magnitude and distribution of traction forces exerted by adherent cells at receptor mediated sites on the substrate to explore the molecular basis for mechano-transduction.

Methods

Polyacrylamide gel preparation and cell culture

Thin films of polyacrylamide (PA) were prepared on functionalized coverslips by modifying previously published protocols to maximize ECM coupling to the gel surface.^{15,16} Briefly, 22 mm glass coverslips (Blue Star) were cleaned by soaking for 15 minutes in 10% solution of 3-amino-propyl triethoxy silane (Sigma Aldrich) and rinsing thoroughly in PBS, incubated in 0.5% gluteraldehyde solution (SDFC Ltd) for 30 minutes, and air dried. Another set of 22 mm glass coverslips were treated with 20 µg ml⁻¹ fibronectin solution (Sigma Aldrich) for 45 minutes and spin coated at 800 rpm with a solution containing 0.2 µm fluorescent beads (Invitrogen) for 5 minutes. The fibronectin coating facilitated homogenous attachment of beads to the coverslip surface. Solutions of acrylamide (40% wt/vol, Sigma Aldrich) and *N,N'*-methylenebisacrylamide (2% wt/vol, Sigma Aldrich) were mixed with distilled water to obtain a 10% acrylamide and 0.1% bisacrylamide gel. PA solution was crosslinked using ammonium persulphate (Sigma Aldrich) and *N,N,N',N'*-tetramethylmethylenediamine (Sigma) to produce gels with Young's Modulus of 10 kPa.¹⁷ 30 µl of the PA solution was pipetted to the bead coated coverslip surface; the activated aminosilane-treated coverslip was next inverted on the gel solution. The coverslips were incubated at room temperature for 30 minutes to permit polymerization. The bead-coated coverslip was next carefully removed and the gels assessed for an even distribution of fluorescent beads using an inverted fluorescence microscope (Leica DMI6000B, Leica Microsystems, GmbH). The PA coated coverslip was finally attached to a 35 mm punched Petri dish (Nunc, ThermoScientific) using a thin layer of vacuum grease (SDFC Ltd) for traction experiments.

A 100 mg ml⁻¹ stock solution of heterobifunctional sulphon-SANPAH linker (ThermoScientific Pierce), diluted 1:200 in HEPES buffer (Sigma Aldrich), was pipetted to the PA surface. The gels were exposed to 365 nm UV light (ThermoScientific) for 10 minutes and washed three times with HEPES buffer. The process was repeated and followed with three washes using HEPES to remove unbound linker from the surface. Fibronectin (100 µg ml⁻¹, Sigma Aldrich) was pipetted and incubated at 37 °C for 45 minutes on the gel surface to allow attachment. The assembly was rinsed twice with PBS to prepare for cell seeding. Mouse embryonic fibroblast (MEF) cells were cultured in a humid environment at 37 °C and 5% CO₂ in DMEM (Sigma Aldrich) supplemented with 10% fetal bovine serum (GIBCO BRL). Cells were seeded at a density of about 2000 cells per ml (total volume 2 ml) on the prepared PA gel and incubated overnight before imaging.

Traction force microscopy using Fourier approaches

PA gels seeded with MEF cells were stabilized for 10 minutes in a live cell chamber mounted on an inverted, fully motorized fluorescence microscope (Leica DMI6000B, Leica Microsystems, GmbH) and images of cells on gels were acquired at multiple positions. Physiological conditions were maintained in the live cell chamber through a temperature controller (PECON, Germany) and regulated gas mixture (5% CO₂, 20% O₂, 75% N₂).

Individual cells were imaged, first using bright field to view the cell boundary and next using fluorescence to characterize the referential bead positions, using an oil immersion objective ($40\times$ with 1.25NA). Imaged cells, selected such that the nearest neighbouring cell was $\sim 80\text{--}100\ \mu\text{m}$ from the centre of the cell under consideration, were next removed from the PA surface using a 2 hour trypsin (2 ml of $10\times$ concentration, Sigma Aldrich) incubation through a custom needle and syringe injection system that did not disturb the motorized stage. The in-plane gel deformation was quantified from marker positions of the reference and deformed images of fluorescent beads using digital image correlation.⁷ Bead displacements were calculated with a starting interrogation window size of 32 pixels \times 32 pixels to a final resolution of 16 pixels \times 16 pixels. These were used as input in the calculation of traction forces on the top surface for all three methods used in this study. We adapted the traction computation algorithm from Butler and co-workers with appropriate input parameters for the gel modulus, Poisson's ratio and the image size as inputs in the FTTC approach.⁷ Specifically, we solve

$$\mathbf{u} = \mathbf{G}\mathbf{t} \quad (1)$$

where \mathbf{u} is the displacement vector, \mathbf{t} the traction vector, and \mathbf{G} is the Green's function for the Boussinesq-Cerruti problem.⁷ We implemented the Reg-FTTC analysis through an Image J plugin using γ values ranging from 10^{-9} to 10^{-11} to examine the influence of regularization parameter (γ) on the computed tractions.¹⁸ In this method, we minimize the expression given below in Fourier space⁹

$$\text{Min}_{\mathbf{t}}\{|\mathbf{G}\mathbf{t} - \mathbf{u}|^2 + \gamma^2|\mathbf{t}|^2\} \quad (2)$$

FE problem formulation and modelling

In the FE method, the PA gel substrate was modelled as a three-dimensional rectangular block of finite dimensions using a Cartesian coordinate system (Fig. 1). We assumed negligible body forces as compared to contractile cellular forces and that tractions exerted by the cell on the top of the substrate were negligible in the normal z -direction as compared to those in the in-plane (x - y) direction. For an isotropic, homogeneous and linear elastic PA substrate in static equilibrium, the governing equations are given in terms of the displacement vector (\mathbf{u}), stress (σ_{ij}) and strain tensors ($\varepsilon_{ij,j}$) as

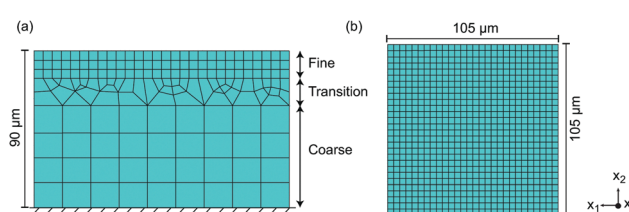


Fig. 1 (a) Geometry and mesh of three-dimensional FE model of the PA gel. Side view shows a graded mesh with fine elements located on the top surface that is in contact with the adherent cell, coarse elements on the bottom, and an intermediate transition zone. (b) A uniform meshing scheme used at the top surface of the gel to compute the cell tractions.

$$\sigma_{ij,j} = 0 \quad (3a)$$

$$\varepsilon_{ij} = \frac{1}{2}(u_{i,j} + u_{j,i}) \quad (3b)$$

$$\sigma_{ij} = \lambda\varepsilon_{kk}\delta_{ij} + 2\mu\varepsilon_{ij} \quad (3c)$$

where the index after the comma represents partial differentiation with respect to that index and δ_{ij} are the components of the Kronecker delta tensor. λ and μ are Lamé's constants and are expressed in terms of the material properties Young's modulus, E (10 kPa), and Poisson's ratio, ν (0.48) as

$$\lambda = \frac{\nu E}{(1 + \nu)(1 - 2\nu)} \text{ and } \mu = \frac{E}{2(1 + \nu)} \quad (4)$$

The boundary conditions specify tractions, \mathbf{t} , at some parts of the substrate boundary and displacements in the remaining parts. We prescribed a mixed boundary condition on the top surface of the substrate, comprising finite in-plane displacements and zero out-of-plane tractions, given by

$$u_x = u_x^*, \quad u_y = u_y^*, \quad t_z = 0 \quad (5a)$$

where (u_x^*, u_y^*) are components of displacements measured on the top surface. We also set zero displacements on the bottom surface of the gel

$$u_x = u_y = u_z = 0 \quad (5b)$$

and zero tractions on the side walls

$$t_x = t_y = t_z = 0 \quad (5c)$$

The governing eqn (3) together with boundary conditions (5) constitute a system of second-order partial differential equations that are solved numerically using the FE method to obtain unknowns in displacements, stresses and strains.

The most widely used FE formulation is displacement-based owing to its simplicity and general effectiveness. Displacements constitute the basic solution variables whereas stresses and strains are obtained as functions of displacements. This formulation however causes significant losses in accuracy, with $\nu \rightarrow 0.5$, for nearly incompressible materials.¹⁹ The deformation obtained is significantly smaller than the actual deformation owing to spurious stresses and the body is said to exhibit volumetric locking. We avoid this singular behaviour in our system by treating the pressure (p) as an independently interpolated solution variable by replacing the constitutive eqn (3c) with

$$\sigma_{ij} = -p\delta_{ij} + 2\mu\varepsilon_{ij} \quad (6)$$

$$\frac{p}{\lambda} + \varepsilon_{kk} = 0 \quad (7)$$

In the incompressible limit, p is interpreted as the hydrostatic pressure, and is given by $p = -\sigma_{kk}/3$. This independent interpolation of pressure term with displacement forms the basis of the mixed (u/p) formulation. We implemented the mixed u/p FE formulation through a commercial finite element software package ABAQUS 6.10 (SIMULIA, Providence, RI). The rectangular block was discretized into finite number of elements connected by nodes. The element type was the

20-noded hybrid hexahedron brick element (C3D20H) with quadratic displacement interpolation, linear pressure interpolation, and full integration at 27 integration points. In-plane displacement data (u_x^* , u_y^*), computed using correlation of deformed and referential bead positions, were prescribed to the nodes corresponding to the top surface of the PA gel domain. These data were subsequently interpolated on mesh refinement to prescribe displacements at the newly generated set of nodes.

Refinement of the substrate domain mesh was achieved through a two-step process. In the first step, we performed an initial run with uniform coarse hexahedron mesh. Successive refinement of this mesh increased the element and node count fourfold which increased the computational costs significantly. To reduce these costs, we used a graded mesh strategy to obtain an initial mesh, M1, which included a fine layer on the top of the domain, an intermediate transition layer in the middle, and a coarse layer at the bottom (Fig. 1a). A small number of wedge elements were used in constructing the transition layer to ensure connectivity between the fine and coarse domains. We selected a C3D15H wedge element type which is a 15-node hybrid element with quadratic displacement interpolation, linear pressure interpolation and full integration at 9 points. In the second step, we obtained graded meshes, M2 and M3, through global refinement of the M1 mesh by successively halving the element length on the top surface. This refinement strategy resulted in a regular set of nodes on the top surface which was common to all three meshes (Fig. 1b) and hence permitted node-by-node comparison between consecutive meshes to assess convergence. Different measures were used to assess convergence of results within an acceptable tolerance from successively refined meshes. Let s_1 , s_2 , s_3 be the stress output obtained for a particular node from meshes M1, M2, and M3 respectively. The relative error in discretization between consecutive meshes M1–M2 and M2–M3, relative to the output of the finest mesh (M3), are given by

$$E_{12} = \frac{s_2 - s_1}{s_3} \quad (8)$$

$$E_{23} = \frac{s_3 - s_2}{s_3} \quad (9)$$

Similar error quantities can be computed for other output measures like maximum stress, average stress, strain energy etc. We set conditions for convergence of results as

$$E_{12} > E_{23} \text{ and } E_{12}E_{23} > 0 \quad (10)$$

The second condition ensures that errors which are oscillatory, for example in cases where E_{12} and E_{23} are of the opposite sign, and diverging, $|E_{12}| > |E_{23}|$, are removed from consideration. For a tolerance, generally set to 10% or 0.1, the results have converged when

$$E_{23} < E_{\text{tol}} \quad (11)$$

Verification approach to computed difference in tractions using simulated data

To verify results from the FE, FTTC, and Reg-FTTC methods, we simulated a simplified loading problem and compared results

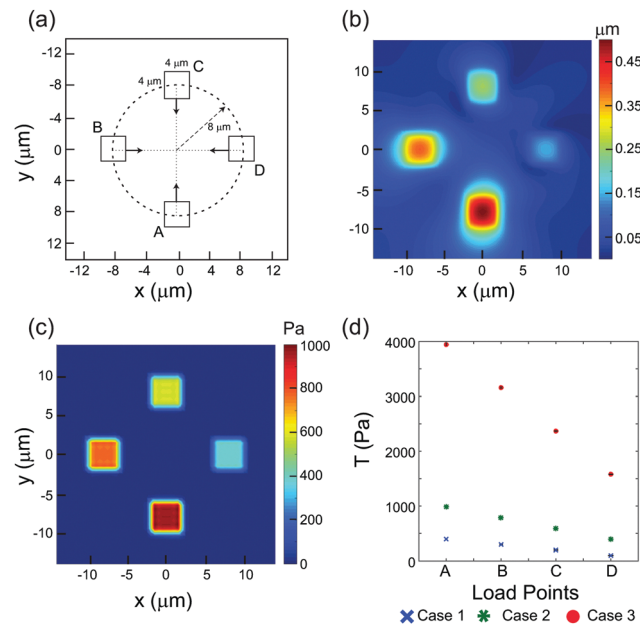


Fig. 2 (a) Schematic representation of the location of load regions. (b) Contour map of displacements obtained using the FE simulation were used as input to FE, FTTC and Reg-FTTC models. (c) Traction contour map of the load region for the prescribed displacements in the FE simulation. (d) Traction reconstructions using the FE method are shown at the load regions A, B, C and D for the test cases corresponding to 400 Pa (Case 1), 1000 Pa (Case 2), and 4000 Pa (Case 3) in the absence of noise.

with the known solution. Specifically, we applied forces of different magnitudes at four symmetrically located regions around a circle located on the top surface of the computational domain, with dimensions of $192 \mu\text{m} \times 192 \mu\text{m}$ and a height of $100 \mu\text{m}$, which corresponded to the PA gel dimensions in the cell traction study (Fig. 2a). Each of these loading regions corresponded to a square region ($4 \mu\text{m} \times 4 \mu\text{m}$) carrying uniformly distributed in-plane loads. The inclusion of four different values of imposed loads at regions A–D in the verification approach is useful to assess sensitivity of the FE and Fourier approaches in computing tractions. We used a graded mesh on the top surface of the gel at the load region to improve the computational efficiency and obtain accurate tractions at the load regions. We first solved for the in-plane nodal displacements on the top surface in the forward approach and used these results as inputs to recover the known forces at the load region in each of the FE, FTTC, and Reg-FTTC methods. Because traction measurements are prone to experimental noise in the displacement data that may be caused by thermal fluctuations, PA gel inhomogeneities and image acquisition limitations, we included a sensitivity analysis in the presence of noise. We assumed that $0.021 \mu\text{m}$ of displacement corresponded to the addition of 50 Pa stress on the gel surface that accounts for 1% noise in the experimental system. We superimposed noise on the displacement data and computed traction stresses and strain energy output using the three approaches.

We used the verification approach to investigate variations in the regularization parameter, γ^* , with maximum traction at

the load region in the presence of displacement noise. Three different cases were investigated in the absence of noise and those with the inclusion of up to 5% displacement noise. Case 1 included application of tractions at the four load regions with varying values from 100–400 Pa to simulate low load conditions. In Case 2, tractions at load regions were varied from 400–1000 Pa to model the average tractions reported to be exerted by most cells. Finally, we included Case 3 from 1600–4000 Pa to investigate the maximum traction effects in the load regions (Fig. 2a).

Results and discussion

Traction force microscopy is a powerful tool to quantify the forces exerted by adherent contractile cells in response to chemical or mechanical stimuli. Multiple methods have been used to compute tractions using experimental measures of substrate deformations by contractile cells. Choice of the method to calculate tractions is however subjective and is based on the availability of computational tools. Few studies have reported differences or assessed the efficacy and sensitivity of the different computational techniques in reporting cellular tractions. A primary goal of this study was to compare differences in the calculated tractions obtained using inverse FTTC and Reg-FTTC approaches and the direct FE method. There are three main implications of this study: first, in the absence of noise, there are no differences in traction reconstructions between all methods. RMS errors are highly sensitive to the magnitude of tractions in the presence of displacement noise. FTTC shows the maximum error in tractions followed by FE method. In contrast, Reg-FTTC method can accurately reconstruct tractions even in the presence of noise. Second, we selected an optimal regularization parameter, γ^* , in the verification study using the maximum curvature of the traction force with variations in γ . This approach is generally suitable to obtain accurate reconstructions for average and high stresses but is unable to accurately predict the low values of tractions. Finally, we compared tractions exerted by MEF cells on 10 kPa gels using the three approaches based on a node-by-node comparison. We show emergence of varying γ^* values for each cell when using the Reg-FTTC approach. Comparisons of the RMS values of tractions from the FTTC method showed ~92% higher values as compared to the Reg-FTTC method and ~22% higher values in the FE method as compared to the Reg-FTTC method.

Comparisons of traction reconstructions from simulated data

Displacements due to applied loads at four symmetrically located regions on the top surface of the computational domain were used to reconstruct tractions using three serially refined meshes, M1 M2 and M3, in the FE method (Fig. 2a). These simulations showed that the stresses converged to the exact solution at the load regions with refinement and included the presence of a border zone region between the loaded and unloaded regions. The strain energy (SE) converged to ~1.6% of discretization error (E_{23}) between the M2 and M3 meshes (Table 1). Fig. 2b shows the displacements which were used as

Table 1 Stress convergence analysis using root-mean-square (RMS) values

Mesh	Element count	T_{\max} (Pa)	T_{RMS} (Pa)	T_{ARMS} (Pa)	T_{RMSA} (Pa)
M1	4373	747.1	121.2	—	—
M2	16 814	1068.6	137.9	16.7	32.5
M3	67 998	1185.4	145.7	7.8	15.9
E_{12} : M1–M2				1.41%	2.74%
E_{23} : M2–M3				0.66%	1.34%

input for the model. A contour map for the reconstructed tractions (Fig. 2c) shows accurate traction reconstructions which were obtained at 0% displacement noise. Within the loading region, the traction values were exact; inclusion of the border region showed small differences between the expected tractions. Lower stresses at the boundary of the loading region occur due to the background effects. We calculated the background noise in tractions using areas outside of the loading regions; the noise in the FE reconstruction method was ~0.001 Pa.

We used three different cases to quantify the differences in traction reconstructions due to low (400 Pa), intermediate (1000 Pa) and high stress (4000 Pa) magnitudes at the loading regions using the FTTC, FE and Reg-FTTC methods (Fig. 2d). The low forces are representative of those exerted at nascent focal adhesion regions^{9,10,20} whereas the intermediate and high forces were based on those exerted by entire cells.^{21–23} Fig. 3a shows plots for variations in the maximum tractions with γ and the corresponding slope-curvature variations for the 3 different test cases in the absence of noise. Comparisons of traction reconstructions show that the optimal value of regularization, γ^* ($=2.3 \times 10^{-12}$), is located at the point of maximum curvature for all cases of low, intermediate and high loads. The maximum traction variations with γ show similar trends as compared to results in the absence of noise with addition of 5% displacement noise. γ^* was identified by an inflection point on the curve.

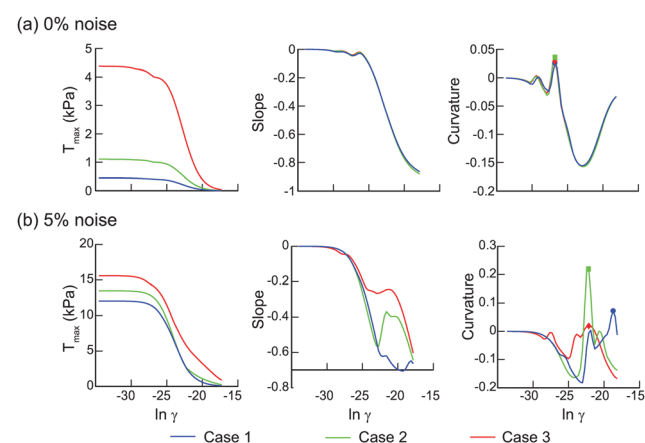


Fig. 3 Maximum tractions corresponding to the three cases were computed for various values of γ in the verification approach using Reg-FTTC. Slopes and curvatures for each of these results are included. (a) Results for the top row, corresponding to 0% noise, have the same γ^* for all cases corresponding to different maximum values of tractions. (b) Results for 5% noise in the displacement data, shown those in the bottom row, have different values of γ^* for these cases.

A finer mesh size through refinement from 0.5 μm to 0.25 μm was warranted to obtain the optimized value in the presence of noise (Fig. 3b). We used the maximum curvature point from these plots to obtain γ^* for each of the three cases and calculated the reconstructed tractions and RMS values in the presence of 5% noise. γ^* has a different value for each of the different test cases in the presence of noise. Comparisons in the presence of 5% noise showed 14% difference in traction reconstructions for the 4000 Pa case when using γ^* at the maximum curvature point as compared to the exact solution value. For the intermediate and low load cases, the variations were 20% and 17% respectively. We selected the intermediate case to compare the traction reconstructions between FE, FTTC and Reg-FTTC methods in the absence of displacement noise.

FE, FTTC and Reg-FTTC methods had the exact values for traction reconstructions in the absence of displacement noise (Fig. 4a). A number of factors may affect the experimentally measured displacements such as changes in imaging conditions and parameters due to thermal fluctuations, local heterogeneities in the marker distributions, and gel formation. We hence assessed the effect of displacement noise in the computed tractions from the different approaches. Earlier methods of incorporating noise used a constant percentage across the entire displacement gradient or used parameters based on the maximum displacement across u_x and u_y in the simulations.^{24,25} A limitation in these approaches is that the addition of noise is a function of the displacement magnitudes which may not be an accurate representation of the actual experimental system. In lieu of this method, we added noise to the displacements such that the standard deviation across u_x and u_y was the same and corresponded to the actual measured background displacements in our experimental system. Results from verification studies show dramatic differences in the presence of noise. The RMS errors, normalized with respect to values for 0% noise (NRMSE), varied by 9.5–25 times for load regions A and D respectively in the FTTC approach for 5% noise. FE results showed differences of 6–16 times under the same loading conditions (Fig. 4a). The FTTC method consistently overestimated tractions at each of the applied load regions in the verification approach. In contrast,

there are few differences in the Reg-FTTC results with regularization regardless of the noise; these were obtained using a different γ^* for each of the different cases in the presence of noise. Traction reconstructions using the Reg-FTTC approach had relatively low values of RMS errors even at 5% noise. Contour map of Reg-FTTC reconstructions shows the ability to reconstruct the domain geometry even in the presence of noise that demonstrates the robustness of this approach (Fig. 4b). Similar verification methods have been employed earlier using either stress-based^{7,9,10,12} or nodal force based criteria¹³ to compare results with known solutions.

Most studies using Reg-FTTC recommend a single value of γ^* for all analyses irrespective of the traction magnitude within the same cell phenotype to reduce averaging of intrinsic cell variations.^{18,20,26} The point force traction reconstruction (TRPF) method uses the L2 regularization method to condition the residual Euclidean norm using the regularization parameter; traction reconstructions are hence prone to errors when computing low values of tractions.⁹ The L-curve criterion^{10,25,27} and χ^2 criterion^{9,28} were previously used to arrive at a subjective choice of γ . Optimal value of γ is obtained from the L curve by locating the point at which the differential between the residual norm and solution norm is maximal. This approach is widely used to compute tractions over a large region of interest, such as an entire cell, using corner finding algorithms to accurately locate γ^* . Stricker *et al.* estimated that γ^* was based on the point preceding the sudden inflection in the output traction values.²⁰

Recent studies demonstrated the shortcomings in using the Tikhonov regularization to determine low force regions at nascent focal adhesion sites.¹⁰ They suggested that use of an L1 regularization in the imposed penalty terms yielded a sparse matrix of tractions which was useful in characterizing the spatial heterogeneity of the reconstructed tractions. An inflection point in the slope-curvature variations of the L-curve represented a high probability region of locating γ^* . This method solved the equations in the spatial domain rather than the frequency domain which makes it computationally expensive. L2 based regularization is hence widely used to compute cellular tractions; however, it is performed using a single value of γ^* . The verification approach used in our study clearly shows that regularization parameter depends on the noise in the measured displacements and loading magnitudes (Fig. 3b and Fig. S1, ESI†). Selection of a single value of γ^* ; in this case the γ_{\max}^* from the 3 cases leads to increased RMS errors in the traction computations (Fig. S1, ESI†). Cellular heterogeneity within the same population is well characterized with respect to differences in the biochemical signalling pathways.²⁹ In case of diseased states like cancer, cellular differences are extremely high due to the cells being in different stages of differentiation, differential access to nutrients *etc.* among other factors.^{30,31} The verification approaches used in this study show that use of a single value of γ^* may hence eliminate these intrinsic differences and thus may not be an accurate representation of the force profile of the cell type.

Quantification of traction forces by adherent cells

Displacement data for MEF cells ($n = 8$) on polyacrylamide gels were used as inputs to the FTTC, FE, and Reg-FTTC approaches.

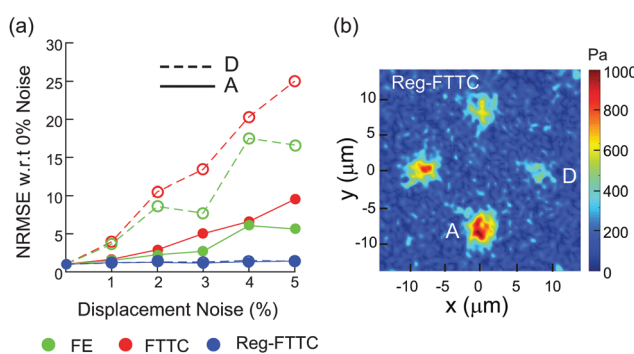


Fig. 4 (a) Normalized RMS errors in the traction reconstructions for the A and D load regions (Case 2) are shown using FTTC, Reg-FTTC, and FE methods in the presence of upto 5% displacement noise. (b) Contour plots at each of the four load regions A–D were computed for Case 2 with 5% noise using Reg-FTTC.

The reaction force output in a displacement-prescribed problem is an exact measure of the tractions that cause these displacements. Reaction forces are distributed among the nodes of the top surface such that they are equivalent to the exerted tractions by the principle of virtual work. The net reaction force and strain energy (SE) for the cell converged rapidly with a final error $E_{23} < 0.3\% (< 0.1\%)$ with mesh refinement. Local measures such as stress converged slowly with finer mesh discretization; this was in contrast to SE and net reaction forces that converged significantly faster. A displacement-based FE formulation does not compute nodal stresses, interpolated and averaged from element integration points, to the accuracy of other output measures such as nodal forces and displacements.¹⁹ A very fine discretization is warranted to establish convergence of local measures such as nodal stress. To assess stress convergence, we compared changes in calculated stress with mesh refinement on a node-by-node basis. An alternate method reported in literature is to compute the average variation in traction measures using root-mean-square (RMS) values.^{12–14} Two such measures may be calculated: first, the $T_{\Delta\text{RMS}}$, calculated as the difference between the RMS value of traction over all nodes (T_{RMS}) between two consecutive meshes. A second measure, T_{RMSA} , is based on the difference in the traction at each node between two consecutive meshes. We computed $T_{\Delta\text{RMS}}$ and T_{RMSA} to assess stress convergence; both measures showed rapid convergence with final errors less than $\sim 2\%$ (Table 1). It is however difficult to estimate the actual stress variation on a nodal level with mesh refinement using globally averaged variations. Other measures that are obtained by normalizing the absolute errors by T_{max} may also be used to assess convergence.

A large part of the domain is relatively unstressed in computing the traction forces in our study. A very small fraction ($\sim 10\%$) of the total nodes located on the surface alone bear high or medium stress. Thus, a significantly large variation in high stresses may appear smaller by averaging over all the nodes in these approaches. We have instead adopted a node-by-node assessment with mesh refinement to assess the overall stress convergence in this work that has not been reported in earlier studies. The M3 mesh was used to obtain tractions from the different approaches. Contour plot showing the magnitude of tractions obtained using FE approach for a representative MEF cell is shown in Fig. 5a. We used in-plane reaction forces on the top surface of the FE domain to generate nodal reaction force maps to quantify and visualize the spatially localized forces exerted by adherent cells (Fig. 5b). Arrows show the direction of traction force at each node; their lengths and colour indicate the magnitude of nodal force that are computed directly from the nodal displacements using the stiffness matrix in the variational approach. Because we used the displacement data on the top surface of the polyacrylamide gel, there is little need to *a priori* assume the location or dimension of the focal adhesions in the FE approach. Localized regions in the cluster are hypothesized to be regions of focal adhesion complexes which are connected to the actomyosin networks and generate contractile forces *via* stress fibers.^{32,33} Approaches like the boundary element method^{9,25} computes tractions using the known area of the focal adhesions. The force map hence

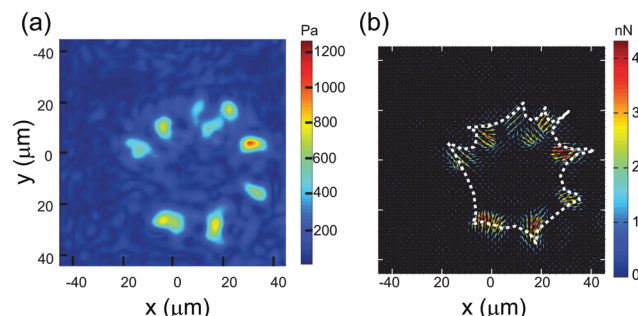


Fig. 5 (a) A contour plot of tractions reconstructions on the top surface of the gel are shown for MEF cell #1 using the FE method. (b) The corresponding nodal force map from the FE simulations show magnitude of the traction forces with vectors showing direction of the force. The cell boundary was added using the Brightfield image of the cell.

provides a visual distribution of contractile stresses in different regions of the substrate that deform the substrate. To date, most published results using traction force microscopy have only used measures, including T_{max} or RMS traction, exerted by adherent cells on substrates as a measure of the cell contractility.

We investigated variations in T_{max} with γ for the MEF cells in our study using procedures outlined in the verification method. A plot of maximum tractions (T_{max}) with γ shows two distinct regions in the curve for each cell: an initial flat plateau region where tractions are insensitive to increase in γ , which is accompanied by a region of steep descent characterized by rapidly reducing tractions (Fig. 6a). γ^* was obtained using the maximum value of curvature of T_{max} with γ in Fig. 6b and corresponded to the inflection point in this plot. In three cells, the inflection point in the curvature plot was not readily identifiable; this warranted mesh refinement from $0.5 \mu\text{m}$ to $0.25 \mu\text{m}$ and next to $0.125 \mu\text{m}$ to identify the inflection point. The values of γ^* range between 1×10^{-13} and 1×10^{-11} for different cells with varying magnitudes of tractions obtained using FTTC (789–1840 Pa) and are given in Table 2. We selected the largest value of γ^* , $\gamma_{\text{max}}^* = 1.77 \times 10^{-11}$, obtained from eight cells and compared the T_{max} results for each specific value of γ^* .

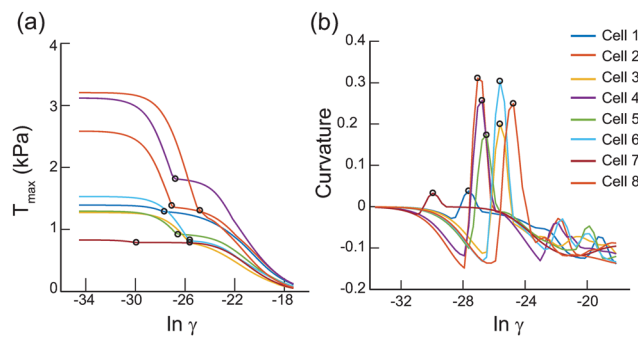


Fig. 6 (a) Variations in the maximum tractions, T_{max} , with γ are plotted for each of the MEF cells in the study ($n = 8$). γ^* values, obtained using the maximum curvature plots, are marked (circle) for each cell. (b) Curvatures using the T_{max} vs. γ plots were calculated and used to obtain γ^* for each cell. We note different γ^* values for each of the different MEF cells in the study.

Table 2 Analysis of optimum regularization parameter (γ^*) in Reg-FTTC for eight MEF cells included in the study

Cell	T_{\max} (FTTC) (Pa)	γ^*	$T_{\max}(\gamma^*)$ (Pa)	$T_{\max}(\gamma_{\max}^*)$ (Pa)	Relative error (%)
0	1299	1×10^{-12}	1286	1189	7.6
1	1382	1.7×10^{-12}	1360	1287	5.4
2	836	7.47×10^{-12}	819	744	9.2
3	1840	2.37×10^{-12}	1817	1745	4
4	940	3.16×10^{-12}	923	887	3.9
6	826	7.47×10^{-12}	815	799	2
7	789	1×10^{-13}	789	766	2.9
8	1310	1.78×10^{-11}	1297	1297	0

for the MEF cells (Table 2). T_{\max} values decreased by ~9% in this comparison (Table 2). In contrast the values did not change significantly upon usage of minimum value of γ^* ; this choice however corresponds to an under-regularized case. The choice of an average or a single value of γ^* may hence result in compromising the accuracy of the traction solution for a given cell type which may lead to errors in using traction values to compare differential cellular responses. Variability in the measured forces exerted by cells may be due to the inherent differences present in individual cells with the same origin and differences in cell cycle phase that were unsynchronized in this study. These variations may also influence the level of regularization essential in obtaining stable solutions. The use of a single regularization parameter also does not account for the inherent biological variability present in cell populations which results in different average forces exerted by the cells on the gel during adhesion. Together, these may lead to significant deviations in the reported traction force profile of cells when using a single value of γ^* . Our study suggests that evaluating γ^* is not a one-step process. Multiple analyses need to be performed to determine an optimum choice of γ^* for each cell using the Reg-FTTC approach.

We used ANOVA with Tukey's HSD (honest significant difference) ($p < 0.001$) to compare differences between the converged node fractions between these methods (Fig. 7a).

Reg-FTTC had a significantly higher fraction of converged nodes (~91%) in the stress measures, followed by 79% for FTTC, and 60% for FE method respectively ($p < 0.001$). We also computed stress convergence fractions for the highest 10% nodes that occur on the top surface in close proximity to the adherent cell and bear a bulk of the maximum load. Comparisons in stress convergence for the top 10% group showed significantly improved convergence for Reg-FTTC and FE (~93% and 75%) in contrast to the FTTC method which showed a drop in convergence to ~44% ($p < 0.001$). That is, a significant fraction of the high stress nodes did not converge in the FTTC method in each of the eight cells as compared to Reg-FTTC which had the highest convergence rate. RMS values of tractions from the FTTC method showed higher values by up to 92% as compared to the Reg-FTTC method (Fig. 7b). RMS values of tractions from FE method also varied by ~22% as compared to the Reg-FTTC method. To assess the role of noise in reported tractions, we defined a traction noise parameter, T_{noise} , using the mean value of stress in remote regions from the cell and compared these values using the three methods. Results from FTTC had the highest value of T_{noise} (~18%) as compared to Reg-FTTC in contrast to ~10% differences obtained between the FE results and Reg-FTTC (Fig. 7b). The values of T_{noise} from FTTC in this work were calculated after exclusion of high traction values located at the domain boundary.

Conclusions

Verification approach in our study shows accurate reconstruction by all three methods in the absence of noise. The FTTC reconstructions had highest errors of ~25 times the actual value with addition of 5% displacement noise for loading region D (400 Pa) corresponding to Case 2 and ~9.5 times for the loading region A (1000 Pa). Elegance of the FTTC method lies in its ease of use and fast computation times. The Reg-FTTC method was highly stable in presence of noisy data but was sensitive to the choice of regularization parameter. In contrast to earlier reports, we show the emergence of varying values of γ^* in our simulated study. Next, we define an inflection point in the T_{\max} vs. $\log \gamma$ curvature curve and show its utility as a good approximation of the optimal γ value. This value can directly be used to compute traction using Reg-FTTC. Earlier studies used visual examination of the traction variations with γ to qualitatively suggest the point preceding the sharp drop in the curve to be used as the optimal value of regularization. The L-optimal, located as a corner point on the L-curve, method in selecting γ^* in the verification method resulted in tractions which were significantly different. The corner point in this method is not easily distinguishable; these comparisons have been reported by Han and coworkers.¹⁰ Other methods like L2 regularization and χ^2 method have also been implemented.²⁸ Choice of the regularization method in reporting tractions is important when comparing the mean or maximum tractions exerted by cells with different cell types or based on chemical perturbations. The method of regularization we suggest is suitable for the measurement of tractions exerted by entire cells; it does not however accurately

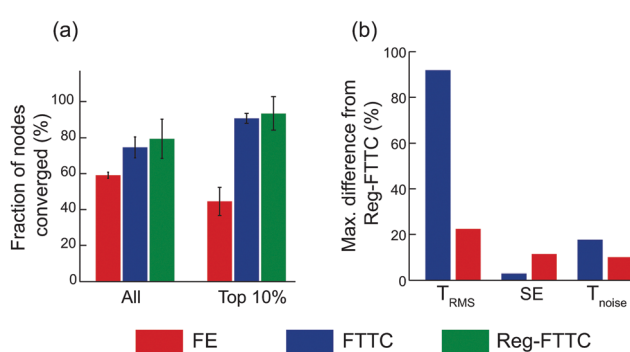


Fig. 7 (a) Converged node fractions were calculated using all nodes in the M3 mesh and those from the top 10% of the maximum stress outputs for the MEF cells using the FE, FTTC and Reg-FTTC approaches. The pairs where the groups are significantly different ($p < 0.001$) are indicated. (b) The maximum difference between results from the Reg-FTTC with FTTC and FE approaches are shown for T_{RMS} , strain energy (SE) and T_{noise} for MEF cells.

represent low tractions exerted at individual focal adhesions. Alternate approaches, such as those based on L1 regularization, may be used in the computation of very low forces such as those at individual focal adhesions. Comparison of experimentally measured displacements exerted by MEF cells show similar trends to that seen in the simulated verification approach. The regularization parameter, γ^* , obtained for each cell using the maximum curvature point was also different in comparison to a single value that is generally used in literature. Using a single value of γ^* led to $\sim 9\%$ variation in the computed maximum tractions within our cell data set. We hence show the need for optimization of γ^* on case-by-case basis rather than a universal value. We considered a subset of nodes that bear high stresses and showed that FTTC had the poorest converged node fractions in contrast to the Reg-FTTC that had the highest. The use of traction cytometry in understanding cellular force generation phenotypes is highly dependent on the method of computation used. This study highlights the differences between the methods and establishes the need for creating a common framework when comparing cell traction force data.

Conflicts of interest

There are no conflicts to declare.

Acknowledgements

We are grateful to Prof. Nagaraj Balasubramanian (IISER, Pune) for the MEF cells used in this study. NG gratefully acknowledges Department of Science and Technology (DST) for the Ramanujan fellowship and research grant that supported part of this work and to the Department of Biotechnology (Bioengineering and Biodesign) for project funding.

Notes and references

- J. C. Del Alamo, R. Meili, B. Alonso-Latorre, J. Rodríguez-Rodríguez, A. Aliseda, R. A. Firtel and J. C. Lasheras, *Proc. Natl. Acad. Sci. U. S. A.*, 2007, **104**, 13343–13348.
- D. A. Lauffenburger and A. Wells, *Nat. Cell Biol.*, 2001, **3**, E110–E112.
- X. Trepaut, M. R. Wasserman, T. E. Angelini, E. Millet, D. A. Weitz, J. P. Butler and J. J. Fredberg, *Nat. Phys.*, 2009, **5**, 426–430.
- C. S. Chen, *J. Cell Sci.*, 2008, **121**, 3285–3292.
- B. Geiger, A. Bershadsky, R. Pankov, K. M. Yamada and B. G. Correspondence, *Nat. Rev. Mol. Cell Biol.*, 2001, **2**, 793–805.
- M. Dembo and Y. L. Wang, *Biophys. J.*, 1999, **76**, 2307–2316.
- J. P. Butler, I. M. Tolić-Nørrelykke, B. Fabry and J. J. Fredberg, *Am. J. Physiol.: Cell Physiol.*, 2002, **282**, C595–C605.
- Y. C. Lin, D. T. Tambe, C. Y. Park, M. R. Wasserman, X. Trepaut, R. Krishnan, G. Lenormand, J. J. Fredberg and J. P. Butler, *Phys. Rev. E: Stat., Nonlinear, Soft Matter Phys.*, 2010, **82**, 1–6.
- U. S. Schwarz, N. Q. Balaban, D. Riveline, A. Bershadsky, B. Geiger and S. A. Safran, *Biophys. J.*, 2002, **83**, 1380–1394.
- S. J. Han, Y. Oak, A. Groisman and G. Danuser, *Nat. Methods*, 2015, **12**, 653–656.
- A. Suñé-Auñón, A. Jorge-Peñas, R. Aguilar-Cuenca, M. Vicente-Manzanares, H. Van Oosterwyck and A. Muñoz-Barrutia, *BMC Bioinf.*, 2017, **18**, 365.
- S. S. Hur, Y. Zhao, Y. S. Li, E. Botvinick and S. Chien, *Cell. Mol. Bioeng.*, 2009, **2**, 425–436.
- X. Tang, A. Tofangchi, S. V. Anand and T. A. Saif, *PLoS Comput. Biol.*, 2014, **10**, e1003631.
- Z. Yang, J.-S. Lin, J. Chen and J. H.-C. Wang, *J. Theor. Biol.*, 2006, **242**, 607–616.
- V. Damljanović, B. C. Lagerholm and K. Jacobson, *Biotechniques*, 2005, **39**, 847–851.
- Y. L. Wang and R. J. Pelham, *Methods Enzymol.*, 1998, **298**, 489–496.
- J. R. Tse and A. J. Engler, *Curr. Protoc. Cell Biol.*, 2010, 1–16.
- Q. Tseng, E. Duchemin-Pelletier, A. Deshiere, M. Balland, H. Guillou, O. Filhol and M. Théry, *Proc. Natl. Acad. Sci. U. S. A.*, 2012, **109**, 1506–1511.
- K.-J. Bathe, *Finite element procedures*, 1996.
- J. Stricker, B. Sabass, U. S. Schwarz and M. L. Gardel, *J. Phys.: Condens. Matter*, 2010, **22**, 194104.
- A. J. Ehrlicher, R. Krishnan, M. Guo, C. M. Bidan, D. A. Weitz and M. R. Pollak, *Proc. Natl. Acad. Sci. U. S. A.*, 2015, **112**, 201505652.
- C. M. Kranning-Rush, J. P. Califano and C. A. Reinhart-King, *PLoS One*, 2012, **7**, e32572.
- A. H. Mekhdjian, F. Kai, M. G. Rubashkin, L. S. Prahl, L. M. Przybyla, A. L. McGregor, E. S. Bell, J. M. Barnes, C. C. DuFort, G. Ou, A. C. Chang, L. Cassereau, S. J. Tan, M. W. Pickup, J. N. Lakins, X. Ye, M. W. Davidson, J. Lammerding, D. J. Odde, A. R. Dunn and V. M. Weaver, *Mol. Biol. Cell*, 2017, **28**, 1467–1488.
- H. Colin-York, D. Shrestha, J. H. Felce, D. Waithe, E. Moeendarbary, S. J. Davis, C. Eggeling and M. Fritzsche, *Nano Lett.*, 2016, **16**, 2633–2638.
- B. Sabass, M. L. Gardel, C. M. Waterman and U. S. Schwarz, *Biophys. J.*, 2008, **94**, 207–220.
- C. M. Perrault, A. Brugues, E. Bazellieres, P. Ricco, D. Lacroix and X. Trepaut, *Biophys. J.*, 2015, **109**, 1533–1536.
- S. V. Plotnikov, B. Sabass, U. S. Schwarz and C. M. Waterman, *High-Resolution Traction Force Microscopy*, Elsevier Inc., 1st edn, 2014, vol. 123.
- R. Merkel, N. Kirchgesner, C. M. Cesa and B. Hoffmann, *Biophys. J.*, 2007, **93**, 3314–3323.
- C. L. Frick, C. Yarka, H. Nunns and L. Goentoro, *Proc. Natl. Acad. Sci. U. S. A.*, 2017, **114**, E2975–E2982.
- U. M. Litzenburger, J. D. Buenrostro, B. Wu, Y. Shen, N. C. Sheffield, A. Kathiria, W. J. Greenleaf and H. Y. Chang, *Genome Biol.*, 2017, **18**, 15.
- A. Nguyen, M. Yoshida, H. Goodarzi and S. F. Tavazoie, *Nat. Commun.*, 2016, **7**, 11246.
- A. Elosegui-Artola, E. Bazellières, M. D. Allen, I. Andreu, R. Oriá, R. Sunyer, J. J. Gomm, J. F. Marshall, J. L. Jones, X. Trepaut and P. Roca-Cusachs, *Nat. Mater.*, 2014, **13**, 631–637.
- P. W. Oakes, S. Banerjee, M. C. Marchetti and M. L. Gardel, *Biophys. J.*, 2014, **107**, 825–833.